

Coherently Controlled Ballistic Charge Currents Injected in Single-Walled Carbon Nanotubes and Graphite

Ryan W. Newson, Jean-Michel Ménard, Christian Sames, Markus Betz, and Henry M. van Driel*

Department of Physics and Institute for Optical Sciences, University of Toronto, Toronto, Ontario M5S1A7, Canada

Received December 18, 2007; Revised Manuscript Received February 12, 2008

ABSTRACT

Ballistic electrical currents are optically injected into aligned single-walled carbon nanotubes and bulk graphite at 300 K via quantum interference between single and two photon absorption of phase-related 700 and 1400 nm, 150 fs pulses. The transient currents are detected via the emitted terahertz radiation. Optical phase and power dependence are consistent with the quantum interference optical process. Under similar excitation conditions, the peak current for a forest of nanotubes, with a diameter distribution of $\sim 2.5 \pm 1.5$ nm, is 9 ± 1 times larger than that in graphite. At peak focused intensities of 10 GW cm^{-2} (1400 nm) and 0.15 GW cm^{-2} (700 nm), the peak current is ~ 1 nA per nanotube. The peak current for pump light polarized along the tubes is ~ 3.5 times higher than that for light polarized perpendicular to the tubes.

Since their discovery in the early 1990s, carbon nanostructures have received considerable research attention because of their unique physical and electronic properties and their potential applications in nanotechnology.¹ In particular, carbon nanotubes and graphene are thought to represent important basic building blocks for future devices because of their unique electron transport properties related to their band structure and low carrier scattering rates. Considerable attention²⁻⁴ has been devoted to electronic transport wherein biased materials are contacted to an external circuit. However, the development of suitable contacts often hinders research in this area. The use of noncontact, optical methods of inducing a current may present opportunities for interfacing photonics and nanoelectronics.^{5,6} Among such methods, optical coherence control has been shown to induce electrical currents in bulk and quantum well materials,⁷⁻¹² that is, three-dimensional (3-D) and two-dimensional (2-D) semiconductors. In such a scheme, quantum interference between optical absorption processes (such as single and two photon absorption) breaks the material symmetry, allowing electrical currents, and, with suitable optical polarizations, even spin currents to be created.¹³ The photocurrent magnitude and direction can be controlled by varying the phase difference between the beams as well as their polarization. A few years ago, Mele and Král,¹⁴ using a tight binding, independent particle model for the electronic bands, predicted that coherently controlled photocurrents could be induced in carbon nanotubes (one-

dimensional, 1-D, conductors), graphene (2-D), and graphite (2-D/3-D) using interference between single and two photon absorption similar to that observed in GaAs, InP, and silicon.^{8,9} To date, experimental confirmation of these ideas is lacking. In this letter, we report observations of coherently controlled photocurrents in a forest of vertically aligned single-walled carbon nanotubes and in bulk graphite. These transient currents are induced using 150 fs, 1400 and 700 nm optical pulses and detected using the emitted terahertz (THz) radiation as a signature. Hence, both the inducing and the probing techniques are noncontact, while the pumping wavelength of $1.4 \mu\text{m}$ lies close to that of technologically relevant sources.

Graphene is a single layer of carbon atoms in a hexagonal lattice. Graphite is the three-dimensional bulk material composed of stacks of graphene sheets bonded with van der Waals forces. While graphite is a semimetal, graphene is a zero-gap semiconductor with a linear dispersion relation for carriers around the K and K' points in reciprocal space. Graphene has often been used as a pedagogical model¹⁵ for other carbon nanostructures, such as carbon nanotubes. For single-walled carbon nanotubes with a large tube diameter (> 1 nm), the electronic band structure can easily be evaluated from that of graphene, using the band-folding model. The current density generation rate J associated with interference between single and two photon absorption processes of beams at 2ω and ω , respectively, is of the form:^{8,14}

* Corresponding author. E-mail: vandriel@physics.utoronto.ca.

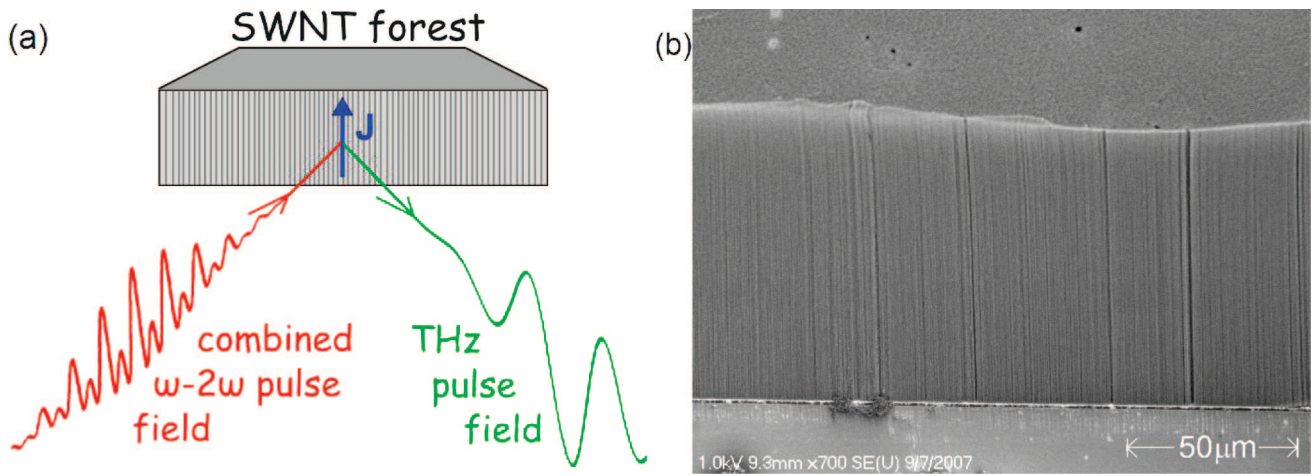


Figure 1. (a) Illustration of sample excitation/terahertz radiation from nanotubes. Beams are separated by nonzero angle for clarity. (b) SEM image of carbon nanotube sample at 45° off-normal, looking at a side facet of the nanotube “forest”.

$$\vec{J} = \vec{\eta} : \vec{E}^\omega \vec{E}^\omega \vec{E}^{-2\omega} \sin(2\phi_\omega - \phi_{2\omega}) \quad (1)$$

where $\vec{E}^{\omega,2\omega}$ and $\phi_{\omega,2\omega}$ are the optical fields and phases, and $\vec{\eta}$ is a fourth rank current injection tensor whose symmetry properties are governed by the illuminated material. This quantum interference process can also be viewed macroscopically as a third order nonlinear optical process.⁸ In the case of graphene, by the simple tight binding model with isotropic bands, the current orientation is predicted to be governed only by the polarizations of the ω and 2ω fields.¹⁴ For carbon nanotubes, a 1-D model predicts¹⁴ the injected photocurrent to be directed parallel (\parallel) to the tube axis, that is, $\eta_{\parallel,\parallel,\parallel,\parallel} \neq 0$, with all other $\eta_{ijkl} = 0$. However, considering the nonzero width of the tubes, additional tensor elements might be nonzero (see below).

For our experiment, a commercial 250 kHz Ti:sapphire oscillator/amplifier operating at 810 nm is used to pump an optical parametric amplifier to produce 150 fs pulses at 1400 nm (ω beam) with an average power, P^ω , up to 30 mW. Part of the ω beam is used with a 1.5 mm thick beta barium borate (BBO) crystal to produce 700 nm light (2ω beam) with $P^{2\omega} = 0.5$ mW. The $\omega/2\omega$ pulses are passed through a two color Michelson interferometer that allows the relative phase, or phase parameter $\Delta\phi = 2\phi_\omega - \phi_{2\omega}$, to be adjusted using piezo control. The two emerging pump beams are copolarized and overlapped on the samples with a $100 \mu\text{m}$ diameter (FWHM) spot size, producing peak focused intensities for the 1400 and 700 nm beams of 10 and 0.15 GW cm^{-2} , respectively. These intensities are well below the damage threshold of the samples as well as the ionization threshold of the ambient air. For a single photon absorption coefficient^{16,17} of $3.2 \times 10^5 \text{ cm}^{-1}$ and a reflectivity of 0.5, the estimated area carrier density in graphite injected by a 700 nm pulse is $N_{2D} \sim 3 \times 10^{11} \text{ cm}^{-2}$. The two photon absorption coefficient is not known for the 1400 nm beam, but if one were to estimate a value of¹⁸ 100 cm/GW, appropriate for bulk materials with a band gap of ~ 1 eV, the injected carrier density is $\sim 2 \times 10^{10} \text{ cm}^{-2}$. There is little data for the linear or nonlinear optical constants for nanotubes, but theoretical estimates indicate that, apart from various spectral features associated with a different density of electronic states, the linear optical absorption coefficient

is close to that of graphite, whereas the two photon absorption coefficient at 700 nm of carbon nanotubes in solution is about¹⁹ 1 cm/MW. Hence, we expect injected carrier densities of $N_{1D} \sim 10^5 \text{ cm}^{-1}$ and $N_{1D} \sim 3 \times 10^4 \text{ cm}^{-1}$ for single and two photon generation processes, respectively.

Measurement of the photocurrent at room temperature is performed noninvasively, by measuring the emitted terahertz radiation.¹⁰ A schematic diagram of the illumination/radiation geometry is shown in Figure 1a. The terahertz radiation emitted by the currents is measured by electro-optic sampling, whereby a weak probe pulse from the Ti:sapphire oscillator at 810 nm is temporally scanned through the terahertz pulse in a $500 \mu\text{m}$ thick (110)-oriented ZnTe crystal.⁹ Because of phase mismatch between the terahertz and the probe beams,²⁰ the effective bandwidth of the electro-optic detection system is estimated to be ~ 3 THz. Complete time resolution of the terahertz pulse or associated current is therefore not obtained; however, the peak electro-optic signal is proportional to the peak current.

The graphite sample is a naturally grown flake, freshly cleaved with scotch tape. The carbon nanotubes are grown by CVD methods²¹ standing vertically and tightly packed (a so-called “forest”) on a Si substrate between 150 and 200 μm in length (see Figure 1b). This is a single-walled nanotube sample; however, a few multiwalled nanotubes may be present. The distribution of the tube diameters is approximately 2.5 ± 1.5 nm. Tube chiralities are randomly distributed within the diameter distributions; both metallic and semiconducting nanotubes are present. Although the fundamental band gaps of the semiconducting tubes in our sample correspond to wavelengths $> 1.5 \mu\text{m}$, there exist many higher energy band gaps between subbands with higher azimuthal quantum numbers. Current injection is therefore expected to be possible in a distribution of nanotubes at almost any photon energy $2\hbar\omega$ well above the fundamental band gaps.

Figure 2 is a contour plot of the terahertz radiation field from the nanotubes as a function of $\Delta\phi = 2\phi_{1400} - \phi_{700}$ and the time delay between 1400/700 nm pump and 810 nm probe beam. Both pump beams are overlapped on the side

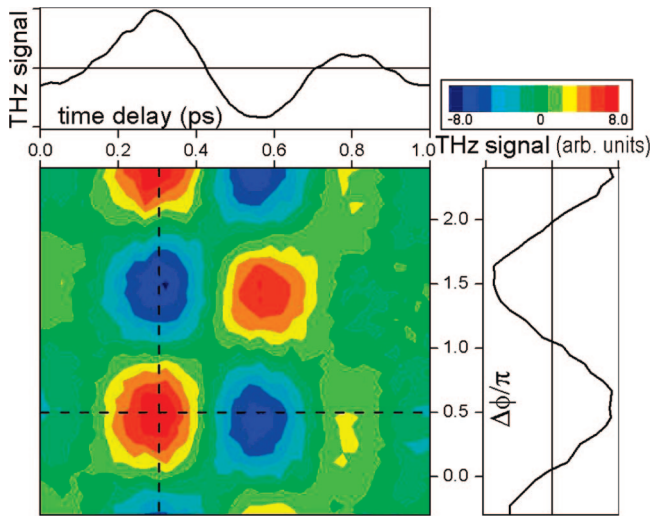


Figure 2. Time dependent terahertz radiation field from the nanotube forest as a function of time delay between 1400/700 nm pump and 810 nm probe pulse and the phase parameter, $\Delta\phi$, between copolarized pump beams. Top panel: terahertz trace time delay dependence for constant $\Delta\phi$ represented by the horizontal dashed line on the contour plot. Right panel: terahertz field $\Delta\phi$ dependence for constant time delay represented by the vertical dashed line on the contour plot.

facet of the nanotube forest and are copolarized with their polarization direction along the tube axes. A typical terahertz pulse trace as a function of probe pulse time delay with constant $\Delta\phi$ is shown in the top panel, corresponding to the horizontal dashed line on the contour plot. The first emission peak at ~ 0.3 ps (see top panel in Figure 2) is followed by a weaker oscillatory trace (only partially shown in Figure 2). As noted above, this oscillatory behavior reflects the limited bandwidth of the terahertz detection scheme²⁰ rather than the intrinsic temporal behavior of the current. Specifically, charge displacement is expected to rise with the 150 fs pulse and decay through the development of space-charge fields and carrier momentum relaxation. The right panel shows the dependence of the terahertz field with $\Delta\phi$ for constant pump/probe delay. The current reverses direction as the phase varies and, more generally, follows a $\sin(\Delta\phi)$ dependence, consistent with the coherently controlled photocurrent description of eq 1. Similar phase dependent current behavior was observed for the graphite sample.

The ratio of the maximum electro-optic signal, or photocurrent magnitude, in the nanotubes to that from graphite is $\sim 9 \pm 1$ with the nanotubes producing a peak current only ~ 10 times less than that observed⁹ in polished, homogeneous GaAs or InP. From the measured peak terahertz amplitude in the nanotubes of ~ 100 V m⁻¹ and a knowledge of the absorption depths in the graphite and nanotube samples, we deduce²² a peak current density ~ 1 kA cm⁻² in the graphite and ~ 10 kA cm⁻² in the nanotubes. Assuming a tube packing fraction of 0.8,²³ the peak current in the tubes is ~ 1 nA. The higher injected current density in the nanotubes compared with that in graphite may reflect a number of factors such as different absorption and reflectivity, or the longer momentum relaxation time,²⁴ and Coulomb enhancement of transition amplitudes in the case

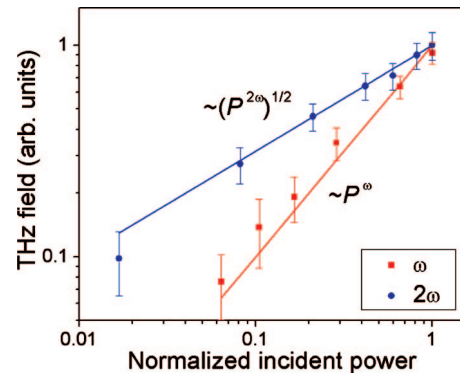


Figure 3. Terahertz radiation magnitude (injected current magnitude) in nanotube sample as a function of ω and 2ω beam average power with the power of the other beam being constant. The solid lines indicate linear and square root power laws.

of the nanotubes.²⁵ Note that no attempt has been made here to maximize the current density by varying the relative power in the two pump beams. In general, the efficiency of current generated is optimal when the number of carriers generated through single and two photon absorption are the same, thereby balancing the two “arms” of the interference process.²⁶ Given graphite’s absorption depth and our signal-to-noise ratio, we do not expect to observe current injection in graphene samples with the present experimental configuration (barring any enhancement effects in the atomically thin films), since the signal from graphene is expected to be about 2 orders of magnitude weaker.

We emphasize that the present technique represents the fastest way to generate charge currents, which can be located wherever one can focus an optical beam and which are not governed by the location or inductance and capacitance effects of electrical contacts. In particular, electrons are photoinjected ballistically; that is, they are injected with a group velocity of the conduction band states into which they are promoted and move thereafter without benefit of an accelerating DC electric field or density gradient. Electrons and holes travel a distance determined by the onset of a space-charge field as electrons and holes separate, or the scattering length which is reported to be ~ 1 μ m at room temperature,³ 2 orders of magnitude larger than in most bulk semiconductors.

To further verify that the terahertz radiation signal is associated with the two color current injection process, we measured the scaling of current generation in the nanotubes with average pump power ($P^{\omega,2\omega}$) of one beam with the power of the other beam being kept constant. From eq 1, we expect $J \propto P^{\omega}(P^{2\omega})^{1/2} \sin(\Delta\phi)$. The experimental data in Figure 3 supports the expected power dependence for both ω and 2ω beams, consistent with the third order optical process.

Anisotropy of the current generation in the nanotubes has been observed by varying the sample orientation relative to pump beam polarization. With the pump beams collinearly polarized, we measured the emitted terahertz radiation along this polarization direction using a terahertz polarizer, while rotating the sample through an angle γ between tube axis

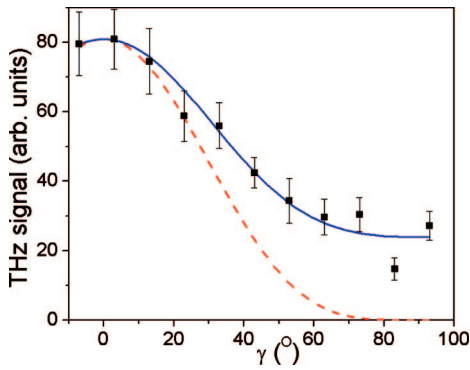


Figure 4. Terahertz amplitude (injected current magnitude) in the aligned nanotubes as a function of γ , the tube axis angle relative to the pump polarization direction. Also shown are theoretical curves for a $\cos^4 \gamma$ fit (dashed red) and a fit with nonzero $\cos^2 \gamma \sin^2 \gamma$ and $\sin^4 \gamma$ terms (solid blue).

direction and the optical polarization direction. Figure 4 shows that the terahertz field (or injection current) varies with angle γ and is maximized (minimized) when the tubes are aligned parallel (perpendicular) to the pump polarization direction. If the current were to be injected only along the tube direction, according to eq 1 for a true 1-D material, the signal is ideally expected¹⁴ to vary as $\cos^4 \gamma$. However, since the carbon nanotube sample has D_n symmetry, besides the $\eta_{\parallel,\parallel,\parallel,\parallel}$ tensor elements, there are also $\eta_{\perp,\perp,\perp,\perp}$, $\eta_{\parallel,\perp,\perp,\parallel}$, and symmetry related elements, where \perp denotes a direction perpendicular to the nanotube. Hence, the current injection is expected to be of the form $J \propto \eta_{\parallel,\parallel,\parallel,\parallel} \cos^4 \gamma + \eta_{\{\parallel,\parallel,\perp,\perp\}} \cos^2 \gamma \sin^2 \gamma + \eta_{\perp,\perp,\perp,\perp} \sin^4 \gamma$ where $\eta_{\{\parallel,\parallel,\perp,\perp\}}$ represents the sum of the six terms containing two \parallel and two \perp components. The appearance of a nonzero current in the data for $\gamma = 90^\circ$ allows us to deduce $\eta_{\parallel,\parallel,\parallel,\parallel}/\eta_{\perp,\perp,\perp,\perp} = 3.4 \pm 0.4$. From the best fit to the data, we also obtain $\eta_{\parallel,\parallel,\parallel,\parallel}/\eta_{\{\parallel,\parallel,\perp,\perp\}} = 2.9 \pm 0.6$. The existence of a current for optical polarization perpendicular to the tube axis is not unreasonable since the linear dielectric constant (absorption) is predicted to be anisotropic as well.¹⁷ Nonetheless, it is interesting that the coherence control techniques offer the ability to consider carrier transport effects perpendicular to the tube axis, something that contact based techniques cannot do. It is possible that a portion of the current at $\gamma = 90^\circ$ is due to imperfect alignment of some of the tubes in the sample, but from SEM pictures, we estimate the degree of tube alignment to be very good.

In conclusion, we have generated large amplitude coherently controlled electrical currents in single-walled carbon nanotubes as well as somewhat smaller currents in bulk graphite using 1400 and 700 nm, 150 fs pulses. These ballistic currents depend on the relative phase between the pulses, and the current direction can be completely inverted by changing this relative phase. The photocurrent has an optical power dependence consistent with a third-order nonlinear optical process. Peak currents ~ 1 nA have been generated in the nanotubes. While these preliminary results are encouraging for all-optical generation of electrical

currents in carbon nanotubes, whereby known methods of synthesis lead to a distribution of tube diameters and a mixture of metallic and semiconducting tubes, future work will consider more defined tube types, the role of excitation wavelength, and the time-resolved behavior. Injecting and coherently controlling photocurrents in graphene is also being considered but may require detection schemes other than terahertz radiation detection. Overall, these experiments may bring new understanding to optoelectronic functionalities in carbon nanomaterials.

Acknowledgment. We are grateful to Paul Finnie, National Research Council (Ottawa, Canada), for providing the vertically aligned single-walled nanotube sample and to NSERC for financial support. J.-M.M. acknowledges additional support from the Walter C. Sumner Foundation.

References

- (1) Huang, L.; Zhang, J.; O'Brien, S. *J. Mater. Chem.* **2007**, *17*, 3849.
- (2) Cottet, A.; Kontos, T.; Sahoo, S.; Man, H. T.; Choi, M.-S.; Belzig, W.; Bruder, C.; Morpurgo, A. F.; Schönenberger, C. *Semicond. Sci. Technol.* **2006**, *21*, S78.
- (3) Purewal, M. S.; Hong, B. H.; Ravi, A.; Chandra, B.; Hone, J.; Kim, P. *Phys. Rev. Lett.* **2007**, *98*, 186808.
- (4) Heersche, H. B.; Jarillo-Herrero, P.; Oostinga, J. B.; Vandersypen, L. M. K.; Morpurgo, A. F. *Nature* **2007**, *446*, 56.
- (5) (a) Franco, I.; Shapiro, M.; Brumer, P. *Phys. Rev. Lett.* **2007**, *99*, 126802. (b) Kohler, S.; Hänggi, P. *Nat. Nanotechnol.* **2007**, *2*, 675.
- (6) Pershin, Y. V.; Piermarocchi, C. *Phys. Rev. B* **2007**, *75*, 035326.
- (7) Dupont, E.; Corkum, P. B.; Liu, H. C.; Buchanan, M.; Wasilewski, Z. R. *Phys. Rev. Lett.* **1995**, *74*, 3596.
- (8) Haché, A.; Kostoulas, Y.; Atanasov, R.; Hughes, J. L. P.; Sipe, J. E.; van Driel, H. M. *Phys. Rev. Lett.* **1997**, *78*, 306.
- (9) Costa, L.; Betz, M.; Spasenović, M.; Bristow, A. D.; van Driel, H. M. *Nature Physics* **2007**, *3*, 632.
- (10) Côté, D.; Fraser, J. M.; DeCamp, M.; Bucksbaum, P. H.; van Driel, H. M. *Appl. Phys. Lett.* **1999**, *75*, 3959.
- (11) Duc, H. T.; Meier, T.; Koch, S. W. *Phys. Rev. Lett.* **2005**, *95*, 086606.
- (12) Marti, D. H.; Dupertuis, M.-A.; Deveaud, B. *Phys. Rev. B* **2005**, *72*, 075357.
- (13) (a) Stevens, M. J.; Smirl, A. L.; Bhat, R. D. R.; Najmaie, A.; Sipe, J. E.; van Driel, H. M. *Phys. Rev. Lett.* **2003**, *90*, 136603. (b) Hübner, J.; Rühle, W. W.; Klude, M.; Hommel, D.; Bhat, R. D. R.; Sipe, J. E.; van Driel, H. M. *Phys. Rev. Lett.* **2003**, *90*, 216601.
- (14) (a) Král, P.; Tománek, D. *Phys. Rev. Lett.* **1999**, *82*, 5373. (b) Mele, E. J.; Král, P.; Tománek, D. *Phys. Rev. B* **2000**, *61*, 7669.
- (15) Dresselhaus, M.; Dresselhaus, G.; Avouris, P., Eds. *Carbon Nanotubes: Synthesis, Structure, Properties and Applications*; Springer: Berlin, 2001.
- (16) Borghesi, A.; Guizzetti, G. *Handbook of Optical Constants of Solids*; 1991, *Volume II*, pp 449–460.
- (17) Guo, G.; Chu, K. C.; Wang, D.-S.; Duan, C.-G. *Phys. Rev. B* **2004**, *69*, 205416.
- (18) Wherrett, B. S. *J. Opt. Soc. Am. B* **1984**, *67*.
- (19) Kamaraju, N.; Kumar, S.; Sood, A. K.; Guha, S.; Krishnamurthy, S.; Rao, C. N. R. *Appl. Phys. Lett.* **2007**, *91*, 251103.
- (20) Gallot, G.; Grischkowsky, D. *J. Opt. Soc. Am. B* **1999**, *16*, 1204.
- (21) Zhang, L. *Chem. Phys. Lett.* **2006**, *422*, 198.
- (22) Côté, D.; Sipe, J. E.; van Driel, H. M. *J. Opt. Soc. Am.* **2003**, *20*, 1374.
- (23) Meakin, P.; Jullien, R. *Europhys. Lett.* **1991**, *14*, 667.
- (24) Xu, S.; Cao, J.; Miller, C. C.; Mantell, D. A.; Miller, R. J. D.; Gao, Y. *Phys. Rev. Lett.* **1996**, *76*, 483.
- (25) (a) Korovyanko, O. J.; Sheng, C.-X.; Vardeny, Z. V.; Dalton, A. B.; Baughman, R. H. *Phys. Rev. Lett.* **2003**, *92*, 017403. (b) Dukovic, G.; Wang, F.; Song, D. H.; Sfeir, M. Y.; Heinz, T. F.; Brus, L. E. *Nano Lett.* **2005**, *5*, 2314.
- (26) Haché, A.; Sipe, J. E.; van Driel, H. M. *IEEE J. Quantum Electron.* **1998**, *34*, 1144.

NL073305L